



Assessment of international standard provisions on stiffness of reinforced concrete moment frame and shear wall buildings



Jinhan Kwon^{a,*}, Wassim M. Ghannoum^b

^a Samsung Economic Research Institute, 4, Seocho-daero 74-gil, Seocho-gu, Seoul 06620, South Korea

^b The University of Texas at San Antonio, One UTSA Circle, Building: BSE 1.202, San Antonio, TX 78249, USA

ARTICLE INFO

Article history:

Received 7 July 2015

Revised 12 June 2016

Accepted 14 September 2016

Keywords:

Concrete
Building
Stiffness
Full-scale
Shaking table
Moment frames
Shear walls

ABSTRACT

The accuracy of the lateral stiffness provisions of international standards is examined for concrete buildings. The stiffness provisions of American, Japanese, Canadian, New Zealand, and European standards are evaluated. Standard stiffness estimates are compared with the experimentally derived lateral stiffnesses of a four-story, full-scale, reinforced concrete building tested under multi-directional seismic motions on the Japanese E-Defense shaking table. The structure was designed to Japanese seismic design requirements and met most U.S. design requirements for regions of high seismicity. The building had moment frames resisting lateral loads in one direction and shear walls in the other. Building stiffness was found to degrade substantially with increasing lateral drifts and relate to prior deformation history. In general, standard stiffness values were higher than those of the building. Standard provisions produced more accurate stiffness estimates for frame members than for walls. All standard provisions produced substantially larger stiffness estimates than experimental values for shear walls. Study results therefore indicate that improvements in the stiffness provisions of all investigated standards for concrete buildings may be warranted.

© 2016 Elsevier Ltd. All rights reserved.

1. Introduction

Structural analysis is an integral part of the design process and its accuracy is essential to achieving safe seismic designs. Particularly, structural stiffness plays a crucial role in determining the natural periods of structures, from which seismic demands ensue. Yet the numerous recommendations found in the literature and design standards around the world provide drastically different recommendations for evaluating the stiffness of structural members and systems. This is especially true for reinforced concrete structures, in which cracking in the concrete generates significant stiffness degradation even at relatively low deformation levels. Given the wide range of stiffness recommendations, it is no surprise that blind prediction contests result in predictions of structural strength and deformations that are several times higher or lower than experimental results [1,2].

At the heart of the issue is the complexity of the stiffness degradation of reinforced concrete members related to concrete cracking and the slip of longitudinal bars in foundations and joints [3,4]. Moreover, the vast majority of experimental tests, on which stiff-

ness recommendations are based, were conducted pseudo-statically on individual structural components. Limited data is available from dynamic tests and tests on complete structural systems, in which member interactions and boundary conditions affecting longitudinal bar-slip are realistically reproduced.

A full-scale, four-story, reinforced concrete (RC) building was tested under multi-directional seismic excitations of increasing amplitude on the National Research Institute for Earth Science and Disaster Prevention (NIED)/E-Defense shaking table in Japan in December of 2010. A two-bay moment-frame system was adopted in the longer plan direction, and a pair of multi-story planar shear-walls were incorporated in the exterior frames in the shorter direction. The building was designed to the modern seismic design requirements of Japan and reflected closely the latest United States (U.S.) seismic provisions for regions of high seismic risk [5,6]. The test series is unique in that no other experiments in the literature involved a full-scale complete structural system of a building designed according to modern seismic design standards, and tested under multi-directional seismic motions, including vertical excitations.

The stiffness provisions of U.S., Japanese, Canadian, New Zealand, and European standards were evaluated in light of experimental data. Stiffness comparisons between standard values and experimental ones were performed at various stages in the loading

* Corresponding author.

E-mail addresses: jinhan.kwon@samsung.com (J. Kwon), wassim.ghannoum@utsa.edu (W.M. Ghannoum).

protocol as the amplitudes of ground motions imparted on the test structure increased. Linear elastic three-dimensional models of the test building were generated in accordance with each of the standards considered, and model lateral stiffnesses were compared with experimental results at each story.

2. Test building details

The plan and framing elevations of the test building are shown in Fig. 1. A moment frame system was adopted in the Frame Direction with two spans of 7.2 m. A pair of multi-story planar walls were incorporated in the Wall Direction within a span of 7.2 m. Walls were coupled to the corner columns by 300 mm deep beams. The thickness of the slab was 130 mm. The story height was 3 m for all stories. The frames in the building were nominally identical in design and detailing. The shear walls at axes A and C contained the same amount of longitudinal reinforcement but differed in the spacing of transverse reinforcement confining the boundary regions. Equivalent lateral forces used to design the building in both directions summed to 20% of the building weight at the base

and were distributed vertically in accordance with AIJ (2010) provisions [7] (Nagae et al. [6]). Building floor weights were estimated at 867 kN, 872 kN, 867 kN, and 934 kN at the 2nd floor, 3rd floor, 4th floor, and roof, respectively.

The measured concrete compressive strengths and moduli of elasticity of the 1st story and 2nd floor, the 2nd story and 3rd floor, the 3rd story and 4th floor, and the 4th story and roof were 39.6 MPa (32.9 kN/mm²), 39.2 MPa (32.8 kN/mm²), 30.2 MPa (30.3 kN/mm²), and 41.0 MPa (30.5 kN/mm²), respectively. The measured yield strengths of the D10 (10 mm nominal diameter), D13, D19, and D22 steel bars were 388 MPa, 372 MPa, 380 MPa, and 387 MPa, respectively. Dimensions and reinforcement details of members are shown in Table 1. The longitudinal reinforcement ratios were moderate and ranged from 1.2% to 1.5% in the columns, and 1.2–2.2% in the beams (Table 1). Axial load ratios due to gravity loads were relatively low and ranged between 0.9% and 7.5% for columns and were 0.2–1.0% for walls (Table 2). The axial load ratio is the applied axial load divided by the member gross sectional area and measured concrete compressive strength. Gravity axial loads were estimated on vertical members based on floor tributary areas and member self-weight.

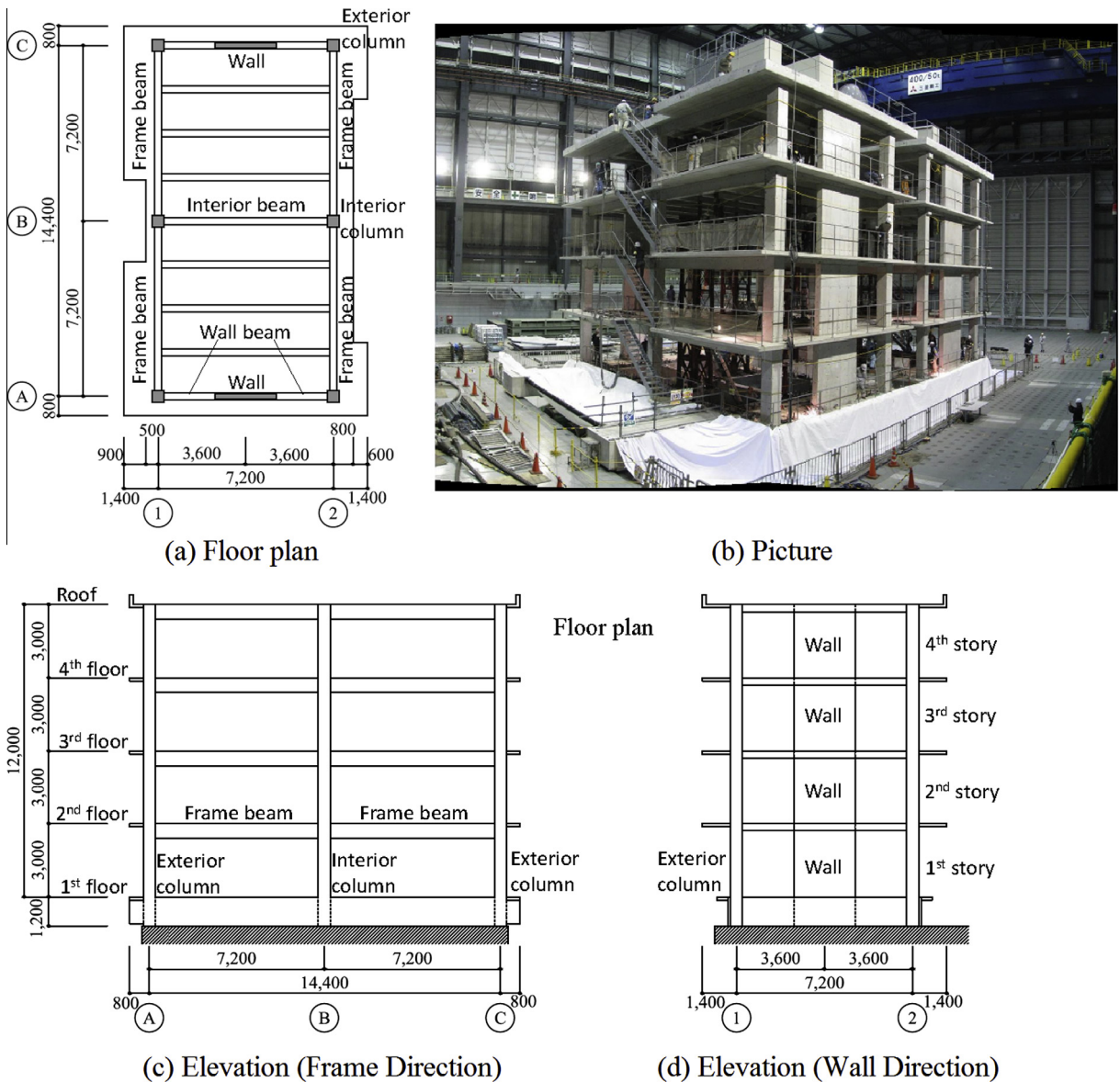
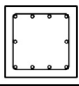
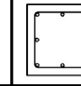


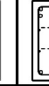

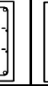



Fig. 1. Building plan, framing elevations, and picture of the building on the E-Defense shaking table.

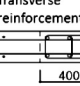
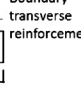
Table 1
Typical dimensions and reinforcement details of members; see [5,6] for more member and reinforcement details.

	Interior columns & 1st story exterior column at the bottom	All other columns
Width x Depth	500 x 500	
Longitudinal reinforcement	10-D22	8-D22
Transverse reinforcement	D10@100	
Reinforcement ratio	1.5%	1.2%
Section		

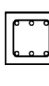
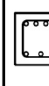


(a) Columns

	2nd floor		3rd floor		4th floor & Roof	
Width x Depth	300 x 600					
Longitudinal reinforcement	End	Center	End	Center	End	Center
	Top	6-D22	3-D22	5-D22	3-D22	4-D22
	Middle	4-D10				
Bottom	3-D22	3-D22	3-D22	3-D22	3-D22	3-D22
Transverse reinforcement	D-10@200					
Reinforcement ratio	1.9%	1.3%	1.7%	1.3%	1.5%	1.3%
Section						

(b) Frame beams

	1st story	Upper stories
Width x Depth	2500 x 500	
Longitudinal reinforcement	2 x 6-D19	
Transverse reinforcement	(A)	D10@125
	(C)	D10@200
Boundary transverse reinforcement	(A)	D10@80
	(C)	D10@100
Section		

(c) Walls

	Lower floors		Roof	
Width x Depth	300 x 300			
Longitudinal reinforcement	End	Center	End	Center
	Top	3-D19	4-D19	3-D19
	Bottom	3-D19	3-D19	2-D19
Transverse reinforcement	D-10@100			
Reinforcement ratio	1.9%	2.2%	1.6%	1.9%
Section				

(d) Wall beams

*Transverse reinforcement layout varies per story
 Note: reinforcement ratio is defined as the area of longitudinal bars divided by the gross area, which can be taken as the section overall height multiplied by the section web width. (Unit: mm)

Table 2
Axial load ratios due to gravity loads on columns and walls.

	Exterior columns (%)	Interior columns (%)	Shear walls (%)
4th story	0.9	2.2	0.2
3rd story	2.5	5.5	0.6
2nd story	2.9	5.8	0.8
1st story	3.8	7.5	1.0

3. Behavior of the test building

The input ground motions applied for the experiments were the JMA-Kobe and JR-Takatori motions recorded during the 1995 Hyogoken-Nanbu earthquake. All components, including the vertical and both horizontal components of the JMA-Kobe ground motion were imparted to the test structure sequentially scaled to 10%, 25%, 50%, and 100% of the original recorded motion. Subsequently, all components of the JR-Takatori motion were imparted scaled to 40% and 60% of the motion. At the end of the test series, the structure had sustained significant damage. The JMA-Kobe motion scaled to 10% did not cause any observable cracking or softening of the structure. The JMA-Kobe motion scaled by 50% was the first motion to generate minor flexural yielding in some members and minor damage in beam-column joints. The seismic motions imparted to the structure beyond the 50% JMA-Kobe motion generated significant inelastic demands and damage. Consequently, this study only explores the effective stiffness of the structure up to the JMA-Kobe 50% test. Figs. 2 and 3 show the acceleration histories and the response spectra for the recorded shaking table motions during the JMA-Kobe 25% and 50% tests. Additional details about the behavior of the test building can be found in Nagae et al. [5,6].

Table 3 presents the maximum drift ratios of the test specimen during the first three seismic motions imparted to it. A story drift ratio is calculated as the lateral drift of the story divided by the story height (3 m), while the roof drift ratio is calculated as the drift of the roof divided by the roof height above the foundation

(12 m). During the JMA-Kobe 25% test, the maximum story drift ratios reached were smaller than 0.3% in both directions. During the JMA-Kobe 50% test, the maximum story drift ratios reached were 0.55% and 1.72% in the Frame Direction, and between 0.61% and 0.89% in the Wall Direction.

Secant story stiffness values were obtained by joining the lateral drift peaks bracketing each story drift cycle as illustrated in Fig. 4. The experimental story shear forces used to obtain story stiffnesses were estimated using accelerations measured at each floor level and floor mass estimates (Kwon [16]). During the JMA-Kobe 10% motion, no changes in the lateral stiffness of stories were observed. The story secant stiffness histories for all loading cycles are plotted in Fig. 5 for the JMA-Kobe 25% and 50% tests. During the JMA-Kobe 25% test, however, significant decreases in the stiffness of the test building were observed in both Frame and Wall Directions. Story stiffnesses decreased by 33–36% in the Frame Direction and by 41–47% in the Wall Direction from the initial values during that motion (Fig. 5). The maximum roof drift ratios reached were 0.18% in the Frame and 0.19% in the Wall Directions during the JMA-Kobe 25% motion. During the JMA-Kobe 50% test, the decrease in story stiffness was also significant in both directions. At the end of the 50% motion, story stiffnesses had decreased by 64–75% in the Frame Direction and 73–84% in the Wall Direction from their values at the start of the JMA-Kobe 25% test. As seen in Fig. 5, the largest stiffness degradations during the JMA-Kobe 50% test occurred at around 15 s into the motion, when peak accelerations were imparted to the building. After the peak acceleration pulses, story stiffnesses stabilized but did not recover original values. The degradation of the stiffness of the building is also captured in Fig. 6, in which story stiffnesses are plotted versus peak drift ratios for each drift cycle. As can be seen in the figure, the stiffness of each story degrades with increasing lateral drift, but then remains at the reduced level corresponding to the largest prior lateral drift regardless of the subsequent smaller drift levels. As a new maximum drift level is reached, the crack patterns in the structure expand and soften the structure. How-

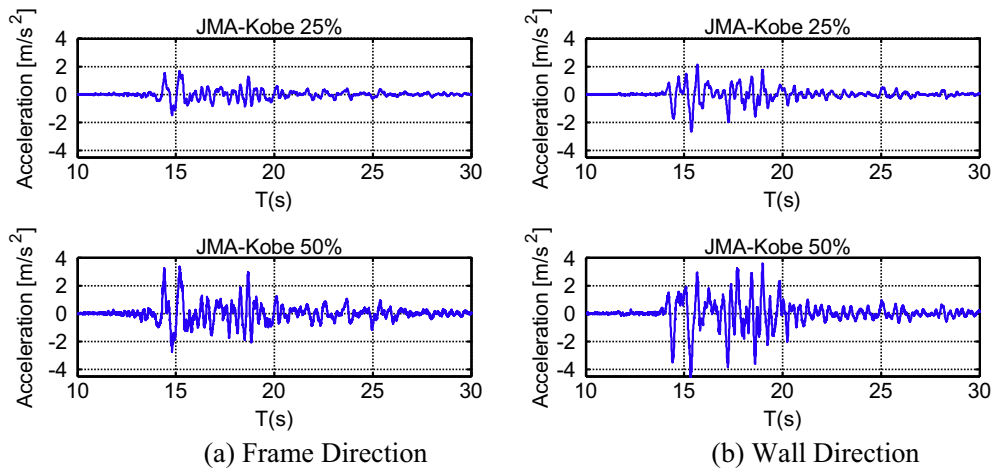


Fig. 2. Acceleration histories of recorded motions at shaking table base.

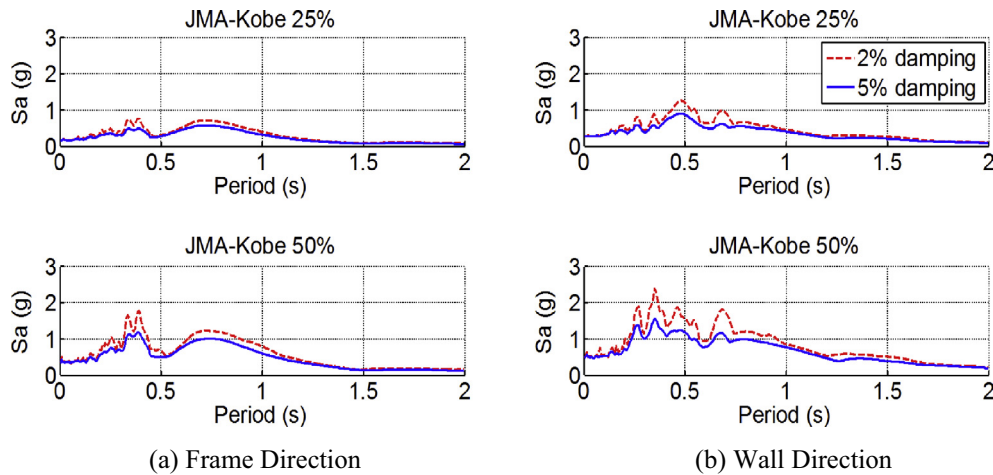


Fig. 3. Acceleration response spectra of recorded motions.

Table 3
Maximum drift ratios.

	JMA-Kobe 10%		JMA-Kobe 25%		JMA-Kobe 50%	
	Frame Direction	Wall Direction	Frame Direction	Wall Direction	Frame Direction	Wall Direction
4th story	0.03%	0.02%	0.10%	0.15%	0.55%	0.61%
3rd story	0.06%	0.04%	0.19%	0.22%	1.10%	0.81%
2nd story	0.07%	0.04%	0.25%	0.22%	1.72%	0.85%
1st story	0.06%	0.03%	0.19%	0.18%	1.46%	0.89%
Roof drift ratio	0.05%	0.03%	0.18%	0.19%	1.18%	0.79%

ever, once cracks have extended during an excursion to a certain drift level, the loss of stiffness associated with the formation of the new crack patterns remains regardless of subsequent excursions to lower drift levels.

4. Evaluation of standard stiffness provisions

It is common for structural engineers to model building structures using a lumped-plasticity approach in which column, beam, and wall members are represented by elastic line-elements having effective stiffness values. Inelastic deformations in such an approach are typically simulated using concentrated hinges at member ends. Structural engineers typically select member effective elastic stiffness values based on provisions of design standards. The stiffness provisions of the following standards were

evaluated in light of the experimental data: (1) Building Code Requirements for Structural Concrete (American Concrete Institute (ACI) Committee 318 2014) [8]; (2) ASCE/SEI 41-13: Seismic Evaluation and Retrofit of Existing Buildings (American Society of Civil Engineers/Structural Engineering Institute (ASCE/SEI) Committee 41 2013) [9]; (3) AIJ 2010: Standard for Structural Calculation of Reinforced Concrete Structures (Architectural Institute of Japan 2010) [7]; (4) CAN/CSA-A23.3-04: Design of concrete structures (Canadian Standards Association 2004) [10]; (5) NZS3101: Part 1:2006: Concrete Structures Standard (Standard Association of New Zealand 2006) [11] and NZS3101: Part 2:2006: Concrete Structures of Standard-Commentary (Standards Association of New Zealand 2006) [12]; (6) Eurocode2: Design of concrete structures (European Committee for Standardization 2004) [13] and Eurocode8: Design of structures for earthquake resistance (Euro-

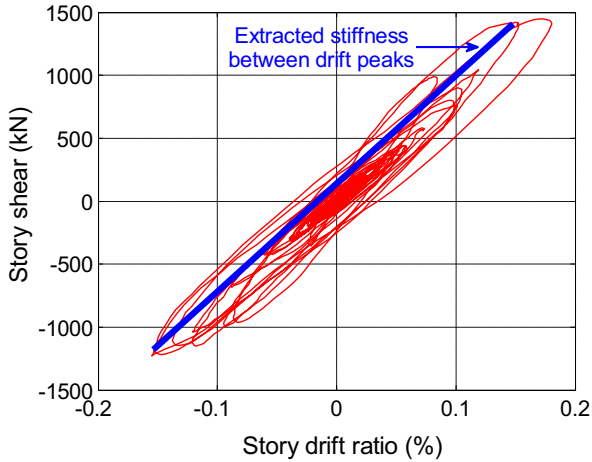


Fig. 4. Illustration of a first-story secant stiffness for a drift cycle during the JMA-Kobe 25% motion (Wall Direction).

pean Committee for Standardization 2004) [14]; and (7) fib 2010: fib Model code for concrete structures 2010 (International Federation for Structural Concrete 2010) [15]. The effective width of slabs acting with beams and the effective stiffness of beams, columns, and shear walls were determined based on the seismic provisions of the standards. Beam-column joints were also modeled as flexible or rigid in accordance with provisions of the standards.

4.1. Three-dimensional computational models

Since test results only provide story stiffnesses and not individual member stiffnesses, a three-dimensional elastic computational model of the structure was built for each standard considered to evaluate standard stiffness provisions. All members were modeled as elastic line elements requiring the definition of the following parameters; (1) the sectional area, (2) the modulus of elasticity, (3) the effective moments of inertia about the strong and weak axes, (4) the shear modulus, and (5) the torsional moment of inertia of the cross section. The gross sectional area (A_g) was used for all elements. The moduli of elasticity used for element definition were the measured moduli of elasticity of concrete (E_c). The effective

moments of inertia (I_{eff}) were input according to each standard's provisions. It is noted that only gravity loads were used when evaluating the effective flexural moment of inertia of vertical members. If the shear modulus was defined in a standard it was used, otherwise the shear modulus was taken as $0.4E_c$. Axial stiffness was based on $E_c A_g$ without reduction for all elements. The gross torsional moments of inertia of cross section were used for all elements.

Since the shear walls were modeled as line elements, essentially rigid beams were introduced to transfer forces from the line elements at the centerline of the shear walls to the connecting beams at wall edges. Rigid truss elements were used to impose an essentially rigid diaphragm constraint at each floor. The truss elements connected all nodes of a floor including mass nodes. Beam-column joints were modeled as rigid members if their stiffness was not defined in the standard considered. Mass was discretized over floor areas to capture the floor mass distribution. Additional detail about modeling assumption can be found in Kwon [16].

The elevation of beam centroids varied in each framing direction due to varying beam depths and effective flange widths. Because lateral loads were resisted primarily by columns and beams in the Frame Direction, the selection of beam centerline heights were more critical in that direction than in the Wall Direction. Therefore, the model was built with all beams and columns intersecting at nodes that are 300 mm below the top of the slab. Mass and stiffness proportional Rayleigh damping was used to assign a damping ratio of 2% to the first and second structural periods. This relatively low damping ratio was used as the structure was bare and did not contain non-structural components that could add to the damping. This value is in line with recommendations by PEER/AT-72-1 [17], Ghannoum and Moehle [3,4], and the Los Angeles Tall Buildings Structural Design Council [18].

4.2. Effective flange width of beams

In the standards considered, the effective flange width of the beams (b_{eff}) is related to the center-to-center span length of the beams (L), the clear span length of the beams (L_{clear}), the slab thickness (h_f), the clear distance to the next parallel beam web ($L_{trans.}$), the beam web width (b_w), and the beam overall depth (h). Span lengths were measured from center to center of the adjacent columns for beams framing into columns at both ends. However,

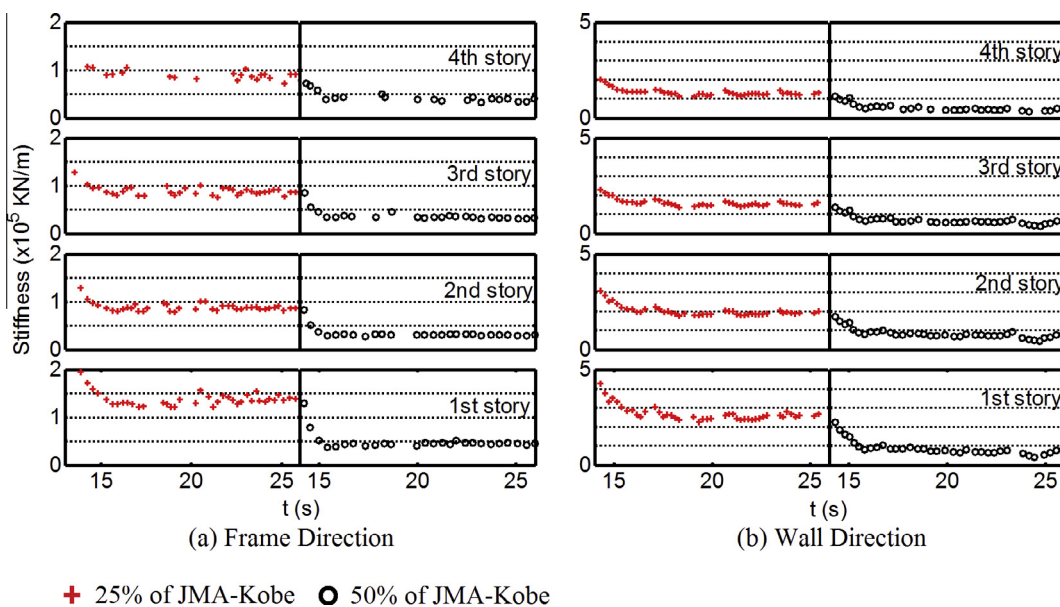


Fig. 5. Story stiffness histories.

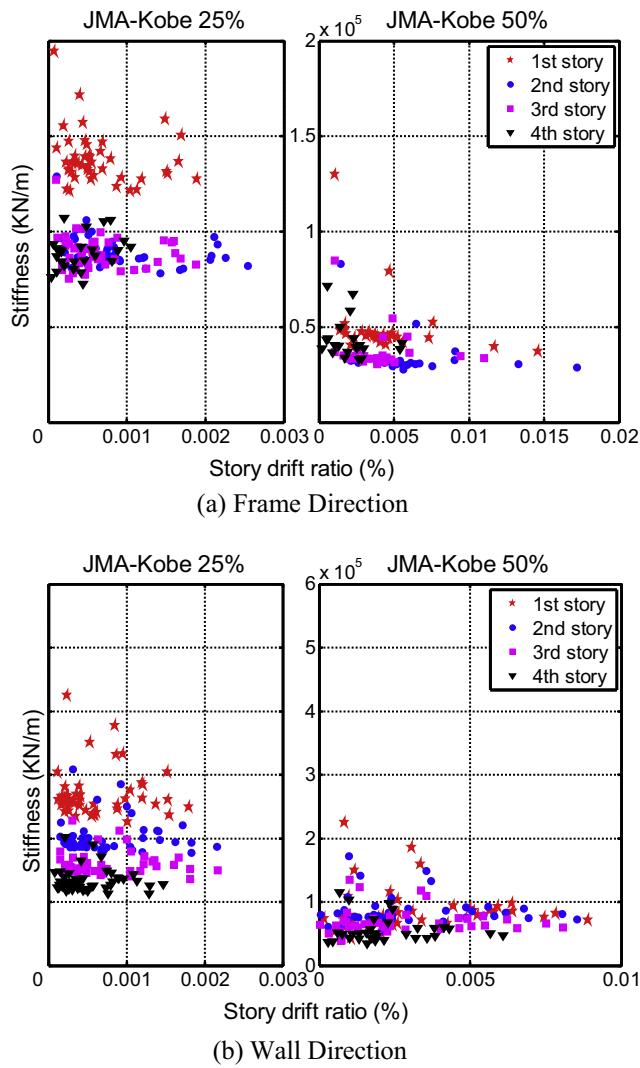


Fig. 6. Story stiffness versus drift ratios of the building.

the span length of beams framing into the corner columns and the walls was taken from the centerline of the columns to the edge of the shear walls. For all exterior beams in both plan directions, one side of the flange was a cantilevered slab (Fig. 1). For those beams, the clear distance to the next web ($L_{cantil.}$) was taken as the length of the overhanging flange on the cantilever side. Table 4 lists the dimensions used in calculating the effective flange widths.

Table 5 lists the equations used to calculate the beam effective flange width (b_{eff}) using ACI 318-14, ASCE/SEI 41-13, CAN/CSA-A23.3-04, and NZS 3101:2006. These standards specify that the lowest value obtained using the equations in Table 5 should be used as the beam effective flange width. In addition to the equations presented in Table 5, NZS 3101:2006 requires the effective flange width on each side of the web not to exceed the clear distance between adjacent beams in the direction considered times the factor of $\frac{1}{2} \left(\frac{h_{b1}}{h_{b1}+h_{b2}} \right)$; where h_{b1} is the beam overall depth and h_{b2} is the overall depth of the adjacent beam.

In AIJ 2010, the effective flange width (b_{eff}) of continuous beams is specified as:

$$b_{eff} = 2(0.1L) + b_w, \quad \text{for } L_{tran} \geq 0.5L \quad (1)$$

where,

L_{trans} : the clear distance to the next parallel beam web,
 L : span length of the beam.

Table 4
Dimensions for the calculation of effective flange widths.

	Frame beams (mm)	Wall beams (mm)	Interior beams (mm)
Span length (L)	7200	2350	7200
Clear span length (L_{clear})	6700	2100	6700
Slab thickness (h_f)	130	130	130
Clear distance to the next web ($L_{trans.}$)	6900	1500	1500
Clear distance to the next web ($L_{cantil.}$) – cantilever slab side	1250	650	N/A
Web width (b_w)	300	300	300
Beam depth (h)	600	300	400

Table 5
Effective flange width (b_{eff}) relations for beams.

ACI 318-14	ASCE/SEI 41-13	CAN/CSA-A23.3-04	NZS 3101:2006
$2(L_{clear}/8) + b_w$	$2(L/5) + b_w$	$2(L/10) + b_w$	$(L/8) + b_w$
$2(8h_f) + b_w$	$2(8h_f) + b_w$	$2(12h_f) + b_w$	$8h_f + b_w$
$\min\{L_{cantil.} + (L_{trans.}/2) + b_w, L_{trans.}/2\}$	$\min\{L_{cantil.} + (L_{trans.}/2) + b_w, L_{trans.}/2\}$	$\min\{L_{cantil.} + (L_{trans.}/2) + b_w, L_{trans.}/2\}$	$h + b_w$

Eurocode2 and fib 2010 allow for a variable effective flange width over the span of a beam. Beams can be split into three sections of varying lengths (l_0) delineated by the flexural inflection points, which can be taken at 0.15 times the center-to-center span of the beam from joint centerlines. In Eurocode2 and fib 2010, the effective flange width for each beam section is specified as:

$$b_{eff} = \sum b_{eff,i} + b_w \leq b \quad (2a)$$

The effective flange overhang on either side of the web is given by:

$$b_{eff,i} = 0.2 \left(\frac{L_{trans.}}{2} \right) + 0.1l_0 \leq 0.2l_0 \quad (2b)$$

The effective flange widths of the end beam sections were therefore smaller than those of the middle beam sections, resulting in a reduced flexural stiffness at beam ends. Table 6 lists beam effective flange widths calculated using the standards considered.

4.3. Element effective flexural rigidities

4.3.1. ACI 318-14 and CAN/CSA-A23.3-04

In ACI 318-14 and CAN/CSA-A23.3-04, the gross-section flexural rigidity, $E_c I_g$, is reduced to obtain the effective flexural rigidity, $E_c I_{eff}$, which accounts for cracking and other softening effects. In accordance with those standards, the gross-section flexural rigidity was reduced in the computational model by a factor of 0.7 for columns, 0.5 or 0.7 for walls, and 0.35 for beams. The flexural rigidity reduction factors for shear walls were determined by comparing

Table 6
Beam effective flange widths (b_{eff}).

	Frame beams (mm)	Wall beams (mm)	Interior beams (mm)
ACI 318-14	1975	825	1800
ASCE/SEI 41-13	2380	1240	1800
AIJ (2010)	1740	770	1740
CAN/CSA-A23.3-04	1740	770	1740
NZS 3101:2006	900	594	700
Eurocode2/fib2010 (beam ends)	732	441	732
Eurocode2/fib2010 (beam mid-span)	2062	909	1608

the wall cracking moment strength, M_{cr} , as defined in each of the ACI 318-14 and CAN/CSA-A23.3-04 standards, to the moment demands obtained from the computational models during the JMA-Kobe 25% or the JMA-Kobe 50% motions. If the estimated moment demands within a story exceeded the cracking moment, a flexural rigidity reduction factor of 0.5 was used, otherwise a factor of 0.7 was used.

It is noted that ACI 318-14 also permits the use of a flexural rigidity reduction factor of 0.5 for all members. However, only the values listed in the preceding paragraph were used in this study when considering ACI 318-14, as the option of utilizing a constant reduction factor of 0.5 was covered when considering Eurocode8 provisions; albeit with slightly different effective flange widths from those specified in ACI 318-14.

4.3.2. ASCE/SEI 41-13

ASCE/SEI 41-13 provisions relate column flexural rigidity to axial load. A rigidity reduction factor of 0.3 was used in the computational model for all columns based on those provisions, as the gravity loads applied to all columns were less than $0.1A_g f_c$. A flexural rigidity reduction factor of 0.5 was used for all shear walls, while it was taken as 0.3 for all beams.

All beam-column joints were modeled by adjusting the stiffness of column and beam offsets within the joint region (joint elements). ASCE/SEI 41-13 provides three options for defining joint element stiffnesses. If the column-to-beam flexural strength ratio is less than 0.8, beam offsets should be rigid and column offsets flexible (i.e., having the stiffness of the adjacent column element). If the column-to-beam flexural strength ratio is between 0.8 and 1.2, half of the beam and column offsets should be rigid and the remaining length flexible. If the column-to-beam flexural strength ratio is larger than 1.2, column offsets should be considered rigid and beam offsets flexible. Column-to-beam flexural strength ratios at all joints of the structure can be found in [6].

Depending on whether moments in beams at corner columns generated tension at the bottom or top of the beams, the column-to-beam flexural strength ratio varied significantly at the end joints and altered the joint-element stiffnesses. Moreover, corner-joint stiffnesses were also influenced by the seismic loading direction that affected column axial loads and consequently flexural strengths. Such a scenario is not treated in the provisions of ASCE/SEI 41-13. In this study, corner-joint column and beam offsets were taken as rigid for half their length and flexible for the other half to arrive at an intermediate joint stiffness that does not change with the direction of lateral loading. Table 7 summarizes the joint element stiffness selections for the test structure in accordance with ASCE/SEI 41-13.

4.3.3. AIJ 2010

AIJ 2010 takes a different approach than U.S. standards and utilizes empirical equations developed by Sugano [19] to define the element effective moment of inertia:

$$I_{eff} = \alpha_y I_g \tag{3}$$

For columns and beams:

$$\alpha_y = \left\{ 0.043 + 1.64np_t + 0.043 \frac{a}{D} + 0.33 \frac{N}{bD\sigma_B} \right\} \left(\frac{d}{D} \right)^2 \tag{4}$$

where,

- I_g : gross moment of inertia,
- b : width of the section,
- D : overall depth of section,
- n : modular ratio of steel to concrete = E_s/E_c (with the steel modulus of elasticity E_s taken as 200,000 MPa),
- p_t : is the longitudinal reinforcement ratio calculated as the area of longitudinal steel divided by the cross sectional area,
- a/D : shear span-to-depth ratio (2.0–5.0),
- N : axial force (positive for compression),
- σ_B : concrete compressive strength,
- d : effective depth of the section measured from extreme compression fiber to the centroid of the flexural tension steel.

In Eq. (4), the axial force term is limited by

$$0.0 \leq \frac{N}{bD\sigma_B} \leq 5.5 \tag{5}$$

For walls:

$$\alpha_y = 0.15 + 0.3p_t \tag{6}$$

4.3.4. NZS3101: Part 1:2006

NZS3101: Part 1:2006 utilizes a similar approach to the U.S. standards and provides simple relations for reducing the flexural rigidity of concrete members. Table C 6.6 in NZS3101: Part 2:2006 was used to calculate the effective rigidity of the members input in the computational model. In the table, stiffness values for concrete members are given depending on the design ductility factor, μ , for a structure. Since this factor is 6 in the Frame Direction and close to 6 in the Wall Direction, as defined in the standard, the stiffness values for that value of μ were selected in this study. The New-Zealand standard relates beam flexural stiffness to the yield strength of longitudinal bars. Column and wall flexural rigidities are also related to the ratio of applied axial load to axial load capacity. A flexural rigidity reduction factor of 0.35 is specified for beams in which the yield strength of longitudinal bars is 300 MPa. A factor of 0.27 applies if the yield strength is 500 MPa. A flexural rigidity reduction factor of 0.32 was used in this study as the yield strength of beam longitudinal bars ranged from 370 to 380 MPa. For columns, the ratio of the gravity axial load to the axial load capacity ranged from 0.9% to 7.5% (Table 2), while the yield strength of longitudinal bars was 370 MPa. Based on these values, the rigidity reduction factors for columns ranged between 0.37 and 0.43. For walls, the ratio of the gravity axial load to the axial load capacity ranged from 0.2% to 1.0% (Table 2), while the yield strength of the longitudinal bars was 380 MPa. Based on these values, the rigidity reduction factors for walls ranged between 0.297 and 0.304. All beam-column joints were modeled as rigid as specified in NZS3101: Part 2:2006.

Table 7

Stiffness selections for joint elements in accordance with ASCE/SEI 41-13.

	Exterior columns		Interior columns	
	Frame Direction	Wall Direction	Frame Direction	Wall Direction
Roof	Rigid beam offset	Rigid column offset	Rigid beam offset	Half column and half beam offsets rigid
4th floor	Half column and half beam offsets rigid	Rigid column offset	Rigid beam offset	Rigid column offset
3rd floor	Half column and half beam offsets rigid	Rigid column offset	Rigid beam offset	Rigid column offset
2nd floor	Half column and half beam offsets rigid	Rigid column offset	Rigid beam offset	Rigid column offset

Note: a joint element was modeled as having the stiffness of the adjacent frame member unless otherwise noted as rigid in the table.

4.3.5. Eurocode8

In Eurocode8, the effective flexural rigidity of all members is given as half of the gross flexural rigidity.

4.3.6. fib 2010

fib 2010 defines the effective flexural rigidity of frame and wall members as the secant value to the yield point. The effective flexural elastic rigidity is obtained in fib 2010 through moment curvature analysis, and accounting for longitudinal bar slip from adjacent members. The effective flexural rigidity is given through:

$$EI_{eff} = \frac{M_y L_s}{3\theta_y} \quad (7)$$

where,

- M_y : yield moment,
- θ_y : chord rotation at member end as given in Eq. (8),
- L_s : moment to shear ratio M/V at member end or the shear span.

It is noted that L_s can be taken as 50% of the clear length of beams and columns. For shear walls, L_s can be estimated as 50% of the height from the base of each story of the wall to the top of the wall in the building.

The yield moments of members were evaluated by sectional analyses at the limit of the elastic range of concrete and steel materials. It was assumed that concrete was essentially linear up to a stress level of $0.7f_c$. The chord rotation at member yielding, θ_y , was obtained as follows:

$$\theta_y = \frac{\phi_y L_s}{3} + \frac{\phi_y d_{bl} \sigma_s}{8\tau_b} \quad (8)$$

where,

- ϕ_y : curvature at yield obtained from sectional analysis,
- σ_s : stress of the longitudinal bars in tension at member end and can be taken as the yield stress of bars,
- d_{bl} : mean diameter of the longitudinal bars in tension,
- τ_b : mean bond stress along the straight anchorage length of the tension bars within adjacent members (e.g., joints or footings).

The mean bond stress is given as $\sqrt{f'_c}$ (MPa) in fib 2010.

The first term in Eq. (8) provides the rotation due to member flexural deformations and the second term provides member rotation due to longitudinal bar slip in adjacent members.

4.3.7. Summary of effective flexural rigidities

Table 8 summarizes the equivalent flexural rigidity reduction factors (α) for all the standards considered ($I_{eff} = \alpha I_g$). ACI 318-14 and CAN/CSA-A23.3-04 provide a constant reduction factor for the effective rigidity of beams and columns, while those factors for shear walls are based on the flexural cracking status of the shear walls. In ASCE/SEI 41-13, the effective rigidity of beams and shear walls are constant, while the reduction factors for columns are based on the applied axial load. In NZS3101:2006, the effective rigidities of structural elements are based on the axial load and yield strength of the longitudinal steel reinforcement. Eurocode8 requires an engineer to use a constant reduction factor

for all flexural elements. fib 2010 provides a method based on sectional analysis, while AIJ 2010 recommends Sugano's empirical equations [19] for determining the flexural stiffness of elements.

5. Stiffness comparison between standards and experiments

The three-dimensional models for each standard were subjected to all components of the JMA-Kobe 50% motion recorded at the foundation of the building. Secant story stiffnesses were extracted from the computational models as was done from experimental data. The average of the model secant story stiffnesses are compared in Fig. 7 with experimental story stiffnesses measured at various testing stages. The experimental and analytical secant stiffnesses shown in Fig. 7 were obtained at the end of each of the JMA-Kobe motions scaled to 10%, 25%, and 50%. For comparison purposes, the cumulative story-stiffness error (CSSE) is defined as the sum of the analytical story stiffnesses divided by the sum of the experimentally derived story stiffnesses (CSS) minus one. Likewise, the first story stiffness error (FSSE) is defined as the analytical story stiffnesses of the first story divided by the experimentally derived first story stiffnesses (FSS) minus one. Table 9 summarizes the experimental cumulative story-stiffnesses (CSS), the experimental first story stiffnesses (FSS), the CSSE, and the FSSE for all standards considered at various stages of the testing protocol.

As can be seen in Fig. 7 and Table 9, no stiffness provisions captured the stiffness of the test building at all lateral drift levels. Standard stiffness values are fixed for given component properties, while the stiffness of the building was observed to decrease markedly as the lateral drifts increased, even at low drift levels (Figs. 5–7). To aid in the comparison between experimental and computational stiffnesses, the secant stiffness values for all lateral drift cycles are plotted in Fig. 8, with arrows linking them in the order the stiffnesses occurred during the JMA-Kobe 50% motion. Fig. 8 highlights the stiffness reductions of the first and second stories with increasing peak prior drift demands. In Fig. 8, the story stiffness values derived using the various standards are introduced as well.

5.1. ACI 318-14 and CSA/CAN-A23.3-04

As can be seen in Fig. 8, ACI 318-14 and CSA/CAN-A23.3-04, which have similar stiffness provisions, produce relatively stiff responses that did not capture test values even at low drift levels. In reinforced concrete frames, yielding of longitudinal bars in beams and columns typically occurs at a lateral drift ratio of about 1% [3,6,21]. Service load levels are typically assumed to generate lateral loads on the order of half to two thirds of the flexural strength of frame members (American Concrete Institute (ACI) Committee 318 2014) [8]. Service load levels therefore correspond to lateral story drift ratios on the order of 0.3–0.7% [20]. Clearly the ACI 318-14 and CSA/CAN-A23.3-04 stiffness provisions for frames produced excessively high stiffness values for the test building, even for service load conditions. In the Wall Direction, ACI 318-14 and CSA/CAN-A23.3-04 provisions produced even greater stiffness errors than in the Frame Direction, with stiffness estimates that are several folds higher than those recorded, even at low drift levels.

Table 8
Reduction factors, α , applied to gross flexural stiffness.

	ACI 318-14	ASCE/SEI 41-13	AIJ 2010	CAN/CSA-A23.3-06	NZS310: 2006	Eurocode8	fib2010
Beam	0.35	0.3	0.23–0.3	0.35	0.32	0.5	0.19–0.25
Column	0.7	0.3	0.23–0.27	0.7	0.37–0.43	0.5	0.19–0.28
Shear wall	0.5–0.7	0.5	0.376	0.5–0.7	0.3	0.5	0.16–0.17

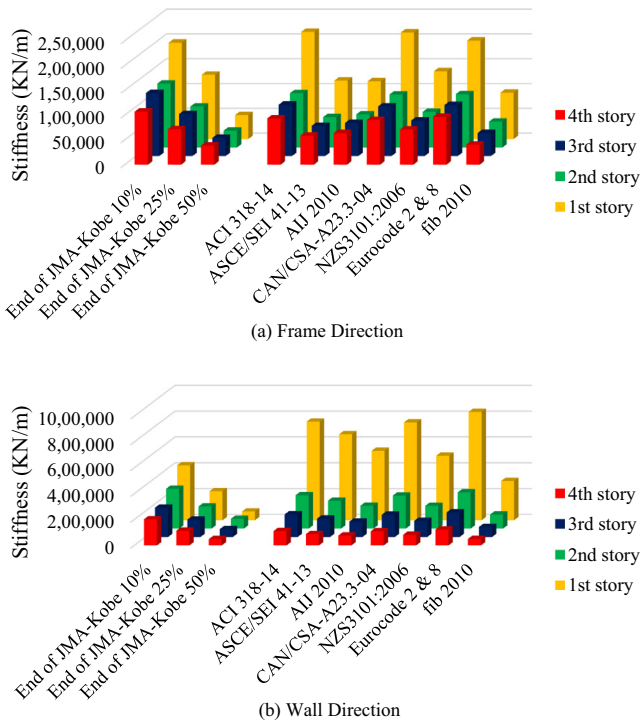


Fig. 7. Stiffness comparisons for each story.

5.2. ASCE/SEI 41-13

In the Frame Direction, ASCE/SEI 41-13 provisions produced story stiffnesses in agreement with the test building values at story drift ratios around 0.19–0.49%, which are in the range of service-load drifts. ASCE 41-13 specifies a fixed flexural rigidity reduction

factor of 0.5 for walls and produced story stiffnesses in the Wall Direction that are significantly over-estimated.

5.3. AIJ 2010

AIJ (2010) produced stiffness values comparable to those of ASCE/SEI 41-13 in the Frame Direction and in closer agreement with experimental results in the Wall Direction. The standard matched experimental story stiffness values at story drift ratios around 0.20–0.40% in the Frame Direction. However AIJ 2010 stiffness provisions produced excessively stiff stories in the Wall Direction compared with experimental results.

5.4. NZS3101: Part 1:2006

Similarly to ASCE/SEI 41-13 and AIJ 2010, the provisions of the New Zealand standard produced story stiffnesses in the Frame Direction in agreement with the test building values at drift ratios around 0.10–0.32%. In the Wall Direction, the New Zealand standard provisions produced stiffness values that are in close agreement with those obtained using AIJ 2010, but too stiff compared with experimental values.

5.5. Eurocodes2 & 8

Eurocodes2 & 8, which utilize the same flexural rigidity reduction factor of 0.5 for all members, produced similar overly stiff stories as the ACI and CSA provisions. Story stiffnesses obtained using the Eurocodes did not match the building stiffness at any drift level.

5.6. fib 2010

In the Frame Direction, the fib 2010 standard produced story stiffnesses that matched experimental values in the drift ratio

Table 9 Standard-based story stiffness errors (best and worst errors highlighted).

		ACI 318-14	ASCE/SEI 41-13	AIJ 2010	CAN/CSA -A23.3-04	NZS3101: 2006	Eurocode 2 & 8	fib 2010
End of JMA-Kobe 10%	FSSE	11%	-39%	-40%	11%	-30%	2%	-52%
	CSSE	-6%	-46%	-44%	-8%	-37%	-9%	-58%
End of JMA-Kobe 25%	FSSE	66%	-9%	-10%	65%	5%	53%	-28%
	CSSE	42%	-19%	-15%	39%	-5%	37%	-37%
End of JMA-Kobe 50%	FSSE	348%	145%	142%	345%	184%	312%	94%
	CSSE	232%	90%	99%	225%	123%	221%	48%
Analytical story stiffnesses(kN/m)	FSS	216,200	118,100	116,6003	215,000	137,000	198,600	93,400
	CSS	523,200	299,600	314,400	512,900	351,800	506,400	232,900

		ACI 318-14	ASCE/SEI 41-13	AIJ 2010	CAN/CSA -A23.3-04	NZS3101: 2006	Eurocode 2 & 8	fib 2010
End of JMA-Kobe 10%	FSSE	80%	57%	26%	78%	17%	97%	-28%
	CSSE	13%	-4%	-22%	11%	-24%	23%	-54%
End of JMA-Kobe 25%	FSSE	240%	196%	139%	237%	122%	273%	37%
	CSSE	103%	72%	41%	101%	37%	122%	-17%
End of JMA-Kobe 50%	FSSE	1,020%	876%	688%	1,010%	632%	1,130%	351%
	CSSE	416%	338%	259%	410%	248%	464%	112%
Analytical story stiffnesses(kN/m)	FSS	763,700	665,700	537,700	757,000	499,610	839,200	307,600
	CSS	1,310,200	1,112,900	911,600	1,296,400	883,900	1,432,800	537,500

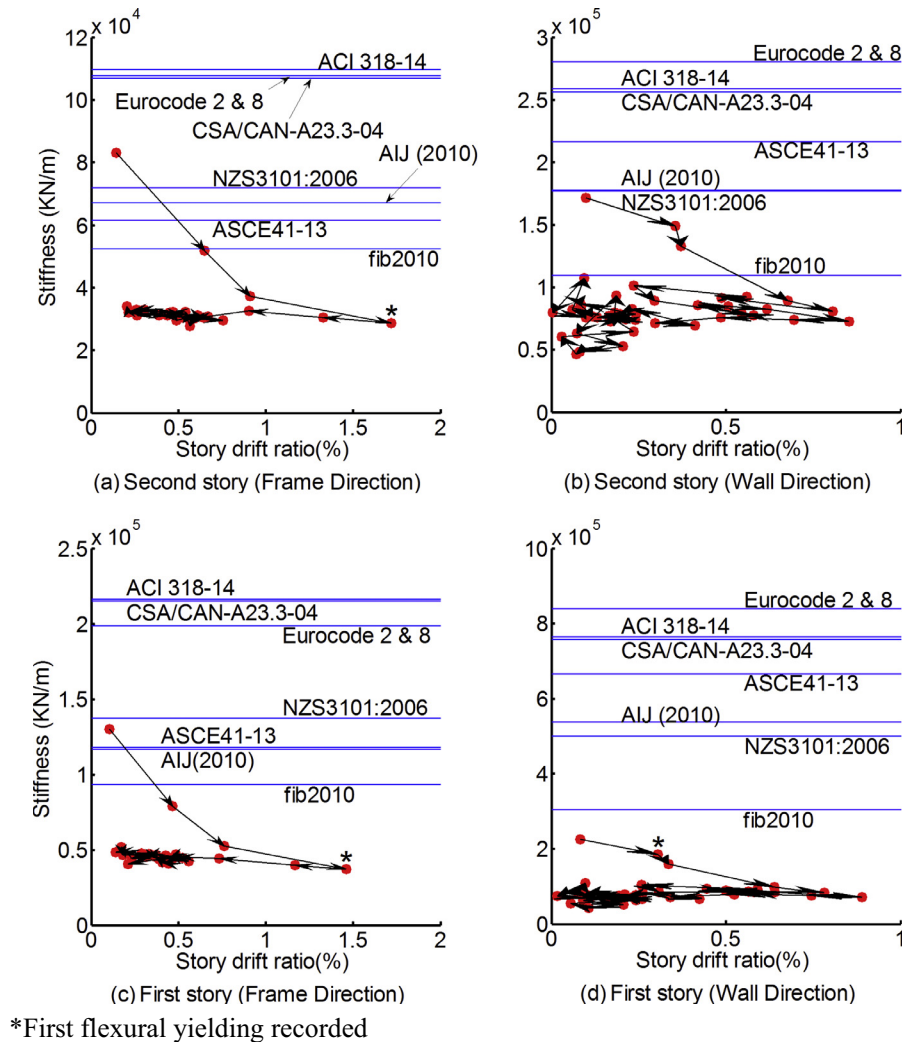


Fig. 8. First and second story stiffnesses versus drift ratios for each cycle of lateral drifts during the JMA-Kobe 50% motion.

range of 0.36–0.64%, which are representative of service level drifts. In the Wall Direction, fib 2010 reproduced the best estimate of story stiffness of all standards, matching second story stiffness at a drift ratio of 0.54% and coming closest to the first story experimental stiffness. The closer match to experimental results may be attributed to the explicit inclusion of reinforcement, axial load, and bar-slip effects at the base of the walls in the fib provisions.

5.7. Stiffness at target deformation level

Each of the design standards used in this study implicitly targets the stiffness of concrete members at a certain deformation level. For example, ASCE/SEI 41-13 stiffness provisions target near-yield deformation levels [22], and come close to that objective for beams and columns but not for walls. Similarly, the provisions of AIJ 2010, NZS3101: Part 1:2006, and fib 2010 used in this study implicitly target near-yield deformation levels and come close in the Frame Direction but not in the Walls Direction. fib 2010 produced story stiffnesses that are closest to those the test structure exhibited at near-yield drift levels.

Some standards define member stiffness values for concrete members at various anticipated deformation demands. The New Zealand standard provides higher stiffness values for concrete members based on a structure's design seismic ductility level. ACI 318-14, on the other hand, allows the increase of the stiffness

values used in this study by a factor of 1.4, if evaluating service-level deflections (ACI 318-14 Section 6.6.3.2.2). However, as indicated previously, the stiffness values obtained using ACI 318-14 provisions without the increase factor were shown to be substantially stiffer than the test values, even at drift levels below what can be deemed service levels. Thus, the increase factor would make the errors worse. Moreover, while the logic of increasing stiffness with decreasing drift levels is justified, it does not account for the loading history of the structure. If a structure was pushed in a previous loading event to near-yield drift levels, then, even at service-level drifts, its stiffness would correspond to the lower levels reached at near-yield drifts. Therefore, applying a factor to member stiffnesses to obtain the stiffness at low deformation demands is not a valid approach. A preferable approach would be to specify the stiffness expected at a given prior peak deformation level and advise engineers to select the stiffness that matches the largest expected prior deformation level for each member. In the absence of prior peak deformation information, it is advisable to bound the solution or use the worst-case stiffness depending on the application. For example, if the peak story drifts are being compared with maximum allowable limits, then assuming that the structure experienced near-yield deformation levels prior to the loading considered and using the associated softer stiffness values would be advisable. If, on the other hand, vibration criteria need to be met, and a stiffer system leads to worse vibrations, then it is

advisable to assume that the structural system experienced limited deformations prior to the loading considered, with associated higher member stiffness values.

6. Summary and conclusions

Experimental results from a full-scale, reinforced concrete building tested under multi-directional seismic motions on the E-Defense shaking table were used to assess the accuracy of stiffness provisions of prominent standards. The building lateral load resistance systems were comprised of moment resisting frames in one direction and planar shear walls in the other. The stiffness provisions of American, Japanese, Canadian, New Zealand, and European standards were evaluated and key observations were as follows:

1. The lateral stiffness of the test structure was observed to decrease significantly at low drift levels. Even at roof drift ratios below 0.18%, story stiffness values were seen to drop by 33–47% from initial values at the start of testing. This is mainly attributed to concrete cracking.
2. Once a story in the building reached a certain peak drift, its stiffness dropped to the stiffness corresponding to that peak drift due to crack expansion, and was never regained regardless of the drift levels experienced below the prior peak. This finding highlights the importance of deformation history on the stiffness of concrete structures.
3. Since design standards considered specify fixed equivalent stiffnesses for concrete members, they could only match test data at a particular drift level (if they matched building stiffnesses at all). Study findings therefore indicate that applying a fixed factor to member gross stiffnesses may not be a valid approach in design. A preferable approach may be to specify the expected stiffness at a given prior peak deformation level and advise engineers to select the stiffness that matches the largest expected prior deformation level for each member. In the absence of prior peak deformation information, it is advisable to bound the solution or use the worst-case stiffness depending on the application and performance objective (i.e., whether force or deformation demands govern).
4. The standards considered captured the building lateral stiffness with varying degrees of accuracy. In general, all standard stiffness values were higher than those of the building at the drift target of the standard.
 - a. fib 2010 produced the most accurate stiffness estimates of all standards in both the Frame and Wall Directions, but still produced overly stiff results especially in the Wall Direction. The higher accuracy of the fib standard compared with others is likely because it bases stiffness estimates on moment-curvature analysis, which explicitly accounts for member axial loads and longitudinal reinforcement ratios.
 - b. ACI 318-14, CSA/CAN-A23.3-04, and Eurocodes2 & 8 produced the largest lateral stiffness errors and did not match the lateral stiffness of the building at any deformation level in both directions. These standards specify fixed flexural rigidity values for members regardless of influential parameters such as axial load or reinforcement details. As such, these standards may match member stiffness at an average set of these parameters. However, given the large influence of the parameters on flexural stiffness, these standards have been shown to produce lateral stiffness estimates that can be several times larger than the measured ones when member parameters differ substantially from the values used to calibrate the provisions. It is noted that the members in the test building were under relatively low axial loads (less than 10% of gross capacity), low shear stresses (0.11–0.32

times the square root of the concrete compressive strength in MPa units), and moderate longitudinal reinforcement ratios (less than 1.5% for all columns and less than 2.0% for all beams within the webs).

- c. AIJ 2010, ASCE/SEI 41-13, and NZS3101:2006 produced lateral stiffness estimates in the Frame Direction matching those of the test structure around service-level drifts, which were higher than the near-yield stiffness values that the standards target implicitly. The standards produced significantly larger stiffness estimates than derived experimentally in the Wall Direction. These standards empirically account, to varying degrees, for influential parameters on lateral stiffness, and may need to be re-calibrated to improve their accuracy.
5. Study results therefore indicate that improvements in the stiffness provisions for concrete buildings of all investigated standards may be warranted, particularly for concrete shear walls.

Acknowledgements

This study was generously funded by the National Science Foundation under Award No. 1201168. Any opinions, findings, and conclusions or recommendations expressed in this material are those of the authors and do not necessarily reflect the views of the sponsor. The authors acknowledge the generous support of the Ministry of Education, Culture, Sports, Science & Technology (MEXT) and of the National Research Institute for Earth Science and Disaster Prevention of Japan for carrying out the tests presented in this paper and generously sharing the test data. The authors gratefully acknowledge Dr. Takuya Nagae for his assistance in analyzing the test data and Drs. Hitoshi Shiohara and Koichi Kusunoki for assistance in navigating the Japanese design standards.

References

- [1] Mahin S, Restrepo J, Buckle I, Schoettler M. Concrete column blind prediction contest 2010; 2010 <http://nisee2.berkeley.edu/peer/prediction_contest/>.
- [2] Bachman R. UCSD, PCA & NEES blind prediction contest; 2006 <http://nees.org/site/annualmeet/4am/docs/J_Restrepo.pdf>.
- [3] Ghannoum MW, Moehle JP. Shake-table tests of a concrete frame sustaining column axial failures. *ACI Struct J* 2012;109(3):393–402. May–June 2012.
- [4] Ghannoum MW, Moehle JP. Dynamic collapse analysis of a concrete frame sustaining column axial failures. *ACI Struct J* 2012;109(3):403–12. May–June 2012.
- [5] Nagae T, Tahara K, Taiso M, Shiohara H, Kabeyasawa T, Kono S, et al. Design and instrumentation of the 2010 E-defense four-story reinforced concrete and post-tensioned concrete buildings PEER Report 2011/104. Berkeley, CA: Pacific Earthquake Engineering Research Center (PEER); 2011. p. 261.
- [6] Nagae T, Ghannoum MW, Kwon J, Tahara K, Fukuyama K, Matsumori T, et al. Design implications of large-scale shake-table test on four-story reinforced concrete building. *ACI Struct J* 2015;112(2):135–46. March–April 2015.
- [7] AIJ. Standard for structural calculation of reinforced concrete structures. Tokyo, Japan: Architectural Institute of Japan; 2010. p. 526 [in Japanese].
- [8] ACI Committee 318. Building code requirements for structural concrete (ACI 318–14)9. Farmington Hills, MI: American Concrete Institute; 2014. p. 524.
- [9] ASCE, SEI Committee 41. Supplement to seismic rehabilitation of existing buildings (ASCE/SEI 41-06). Reston, VA: American Society of Civil Engineers; 2007. p. 428.
- [10] CSA A23.3-04. Design of concrete structures, canadian standards association. Mississauga, ON, Canada; 2004. Pp. 258.
- [11] NZS3101, Part 1:2006. Concrete structures standard: Part 1—the design of concrete structures. Wellington, New Zealand: Standards Association of New Zealand; 2006. p. 309.
- [12] NZS3101, Part 2:2006. Concrete structures standard: Part 2—commentary. Wellington, New Zealand: Standards Association of New Zealand; 2006. p. 298.
- [13] Eurocode 2. Design of concrete structures – Part 1–1: general rules and rules for buildings EN 1992-1-1. European Committee for Standardization; 2004. p. 225.
- [14] Eurocode 8. Design of structures for earthquake resistance – Part 1: general rules, seismic actions and rules for buildings EN 1998-1. European Committee for Standardization; 2004. p. 229.

- [15] fib model code for concrete structures. International Federation for Structural Concrete (fib), V. 1-Bulletin 55, V. 2-Bulletin 56; 2010. 402 pp.
- [16] Kwon J. Strength, stiffness, and damage of reinforced concrete buildings subjected to seismic motions Ph.D. Dissertation. Austin, TX: The University of Texas at Austin; 2016. p. 218.
- [17] Pacific Earthquake Engineering Research Center (PEER) and Applied Technology Council (ATC). Modeling and acceptance criteria for seismic design and analysis of tall buildings. PEER/ATC PEER/ATC 2010;72-1:242.
- [18] Los Angeles Tall Buildings Structural Design Council. An alternative procedure for seismic analysis and design of tall buildings located in the Los Angeles region, Los Angeles, CA; 2014. p. 56.
- [19] Aoyama H, Ito M, Sugano S, Nakata S. A study on the cause of damage to the Hachinohe technical college due to 1968 Tokachi-oki earthquake (Part 1). In: Proceedings of the third Japan earthquake engineering symposium – 1970, Tokyo, Japan; 1970. p. 795–802.
- [20] Ghannoum WM, Sivaramakrishnan B. ACI 369 rectangular column database. Network for Earthquake Engineering Simulation (NEES) 2012. <http://dx.doi.org/10.4231/D36688150>. <https://nees.org/resources/3658>.
- [21] Haselton CB, Liel AB, Deierlein GG, Dean BS, Chou JH. Seismic collapse safety of reinforced concrete buildings. I: Assessment of ductile moment frames. J Struct Eng 2010;137(4):481–91.
- [22] Elwood KJ, Matamoros AB, Wallace JW, Lehman DE, Heintz JA, Mitchell AD, et al. Update to ASCE/SEI 41 concrete provisions. Earthquake Spectra 2007;23 (3):493–523.